

Stark Tuning and Charge State Control in Individual Telecom C-Band Quantum Dots

N.J. Martin,^{1,*} A.J. Brash,¹ A. Tomlinson,¹ E.M. Sala,^{2,3} E.O. Mills,¹ C.L. Phillips,¹ R. Dost,¹ L. Hallacy,¹ P. Millington-Hotze,¹ D. Hallett,¹ K.A. O’Flaherty,^{2,3} J. Heffernan,^{2,3} M.S. Skolnick,¹ A.M. Fox,¹ and L.R. Wilson¹

¹*School of Mathematical and Physical Sciences, University of Sheffield, Sheffield S3 7RH, UK*

²*EPSRC National Epitaxy Facility, University of Sheffield, Sheffield S1 4DE, UK*

³*School of Electrical and Electronic Engineering, The University of Sheffield, North Campus, Broad Lane, S3 7HQ Sheffield, UK*

Telecom-wavelength quantum dots (QDs) are emerging as a promising solution for generating deterministic single-photons compatible with existing fiber-optic infrastructure. Emission in the low-loss C-band minimizes transmission losses, making them ideal for long-distance quantum communication. In this work, we present the first demonstration of both Stark tuning and charge state control of individual InAs/InP QDs operating within the telecom C-band. These QDs are grown by droplet epitaxy and embedded in a InP-based n^{++} - i - n^+ heterostructure, fabricated using MOVPE. The gated architecture enables the tuning of emission energy via the quantum confined Stark effect, with a tuning range exceeding 2.4 nm. It also allows for control over the QD charge occupancy, enabling access to multiple discrete excitonic states. Electrical tuning of the fine-structure splitting is further demonstrated, opening a route to entangled-photon-pair generation at telecom wavelengths. The single-photon character is confirmed via second-order correlation measurements. These advances enable QDs to be tuned into resonance with other systems, such as cavity modes and emitters, marking a critical step toward scalable, fiber-compatible quantum photonic devices.

INTRODUCTION

Photonic quantum technologies promise transformative advances in communication, computation, and sensing. Emerging examples include: quantum key distribution (QKD), linear-optical quantum computing and entangled photon microscopy [1–6]. A critical component of these systems is the ability to generate and manipulate single photons with high purity and coherence, making high-quality single-photon sources (SPS) essential. Semiconductor quantum dots (QDs) have emerged as a leading SPS platform due to their deterministic photon emission, high purity, and strong optical coherence [3, 7, 8]. Unlike spontaneous parametric down-conversion (SPDC) or four-wave mixing (FWM), which rely on probabilistic photon pair generation, QDs provide on-demand emission with near-unity indistinguishability [9–11]. Moreover, QDs can be engineered to operate in the telecom wavelength bands, minimizing fiber losses and enabling long-distance quantum communication [12–20]. Photons in these wavelength ranges exhibit less signal attenuation, with the conventional band, or C-band, representing the minimum of fiber attenuation, as low as 0.15 dB/km for the C-band compared to 3 dB/km for wavelengths < 1000 nm) [8].

In the telecom C-band, QDs have already demonstrated competitive results as single-photon sources [21–26] and entangled-photon sources [27, 28] in un-gated wafers. However, the performance of un-gated QDs is often limited by charge noise and spectral diffusion, where in the absence of an applied electric field, fluctuating charges within the semiconductor matrix induce local electric field variations, leading to spectral wandering and broadening that degrade coherence and so indistinguishability

bility [29–32].

To address these challenges, previous work has explored strategies to reduce charge instability by modifying both the growth mode of the QDs and embedding them in doped heterostructures. Charge noise effects may be influenced by the presence of a wetting layer (such as those present in QDs grown using the Stranski-Krastanov (SK) method) which can act as a reservoir for excess carriers and contribute to spectral fluctuations [29, 33]. In contrast, droplet epitaxy (DE) does not produce a full continuous wetting layer and provides enhanced dot symmetry, which may help mitigate charge noise and contribute to improved spectral stability [33–38]. In addition to growth optimization, gated QD structures embedded in p-i-n diodes or Schottky junctions have also been developed to stabilize the charge environment, suppress spectral diffusion, and enhance photon indistinguishability [17, 23, 28, 39–41]. However, in III-V based semiconductor heterostructures, particularly InP-based QD structures, a significant issue arises from p-dopant diffusion, where elements such as Zn migrate through the heterostructure, leading to unintended charge fluctuations and non-uniform electric fields [23, 32]. This can significantly limit the effectiveness of p-i-n gating strategies in InP-based quantum photonic devices, and may prevent the creation of the thin membranes [42] required for low mode volume cavities and single mode operation within slab waveguides. Additionally, a drawback of p-type dopants is that the low mobility of holes, which is approximately twenty times lower than that of electrons, this can potentially limit high-frequency electrical modulation in p-i-n structures [43, 44]. Moreover, p-type doping introduces roughly twice as much free carrier absorption compared to n-type

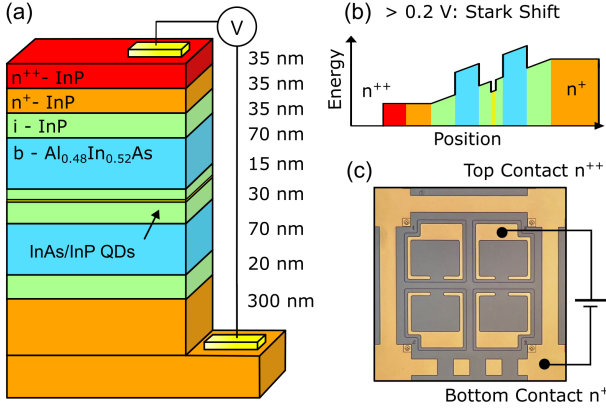


FIG. 1. (a) Schematic of the sample structure. We begin with a 300 nm n-doped InP layer ($2.0 \times 10^{18} \text{ cm}^{-3}$). Next, a 70 nm $\text{Al}_{0.48}\text{In}_{0.52}\text{As}$ barrier is grown to reduce current and block carriers. The intrinsic region then comprises a 35 nm undoped InP spacer, a 1 nm droplet-epitaxy InAs quantum dot layer (for telecom-wavelength emission), and a 15 nm undoped InP capping layer. Another 70 nm $\text{Al}_{0.48}\text{In}_{0.52}\text{As}$ barrier provides electrical isolation. Finally, a 35 nm n^+ InP layer ($2.0 \times 10^{18} \text{ cm}^{-3}$) and a 35 nm n^{++} InP layer ($1.0 \times 10^{19} \text{ cm}^{-3}$) is deposited. (b) Schematic conduction band profile above 0.2 V Gate voltage. (c) Microscope image of fabricated mesa structure (0.14 mm^2), showing the top and bottom contacts.

doping[43, 45], further degrading device performance, such as decreasing cavity quality factors and increasing transmission losses in waveguides.

Recently, similar challenges associated with p-type dopants in GaAs, have motivated the use of n-type only doped structures grown by molecular beam epitaxy (MBE) to tune and control the charge state of near infrared emitting InAs/GaAs QDs [43]. Similarly, to address the p-dopant issues in our work, we introduce an InP $n^{++} - i - n^+$ structure incorporating InAs/InP QDs grown via MOVPE-based droplet epitaxy. This structure enables the application of a precise electric field across the QDs contained within the intrinsic region at the center of the structure. The structure facilitates Stark tuning, provides effective control over the QD charge state, significantly reduces background emission, and consequently improves single-photon purity. Our approach successfully demonstrates pure single-photon emission at telecom wavelengths combined with wavelength tunability ($> 2.4 \text{ nm}$) via the Stark effect, enabling integration into advanced quantum photonic circuits. By implementing n-type-only electric field control, we have effectively mitigated issues related to p-type dopant diffusion in InP, establishing a stable and scalable platform critical for quantum photonics applications.

RESULTS

The layer structure of the device studied here, shown in Fig 1(a), began with the deposition of a 300 nm n-doped InP layer ($2.0 \times 10^{18} \text{ cm}^{-3}$) at 610°C . This was followed by 20 nm of undoped InP. A 70 nm $\text{Al}_{0.48}\text{In}_{0.52}\text{As}$ layer lattice-matched to InP was then deposited, serving as a barrier and current blocking layer, allowing current management and carrier confinement within the active region. Then a 30 nm undoped InP spacer, a central layer of InAs QDs, and a 15 nm undoped InP capping layer was grown. The QDs were grown by DE in MOVPE via the deposition of In droplets, subsequently crystallized by an As flow. For further details on the growth sequence, we refer to our previous work [34, 35]. The intrinsic region was then followed by another 70 nm $\text{Al}_{0.48}\text{In}_{0.52}\text{As}$ layer that again acts as a barrier and current blocking layer, and a further 35 nm of undoped InP. The structure was finalized with a 35 nm n^+ InP layer ($2.0 \times 10^{18} \text{ cm}^{-3}$) followed by a 35 nm n^{++} InP contact layer ($1.0 \times 10^{19} \text{ cm}^{-3}$).

The QD PL intensity presented in Fig.2(a) shows the PL from the wafer under above-band (852 nm) excitation as a function of gate voltage applied. In Fig.2(b), representative spectra from the data presented in (a) at -0.2 V (panel i) exhibit pronounced background emission, whereas at 0.9 V (panel ii) the background is significantly suppressed. We note that the pronounced asymmetry and persistent background emission observed in Figs.2(a-b) may arise from charge accumulating in or around the intrinsic region, which alters the local band profile and leads to an asymmetric, broadened background continuum. Fig.2(c) shows that the average background count rate (over the range 1518.5-1565 nm) under above-band (852 nm) excitation decreases substantially as the gate voltage increases. The reduction in background emission at higher gate voltages correlates with changes in current through the device, as shown by the I-V characteristics shown in Fig.2(d), measured at 4.2 K under $30 \mu\text{W}$ excitation (see Supplementary Section S3 for a more detailed discussion of the I-V characteristics). Using a Hanbury Brown-Twiss setup under CW excitation at 852 nm with a gate voltage of 1.18 V and emission at 1530.3 nm, we confirm the single-photon character of the QDs' telecom-wavelength emission. As shown in Fig.2(e), we observe a raw coincidence minimum of $g^{(2)}(0) \approx 0.18$. Deconvolving the $g^{(2)}(\tau)$ curve (accounting for the finite bin width and instrument response time) yields $g^{(2)}(0) = 0.04 \pm 0.04$. For the same state at the same voltage, time-resolved photoluminescence measurements under pulsed excitation at 830 nm yielded a lifetime of 2.2 ns (see Supplementary Section S4).

Gate voltages not only influence background emission but also enable controlled loading of individual QDs with electrons. Fig. 3(a) shows the QD PL, mapped as a

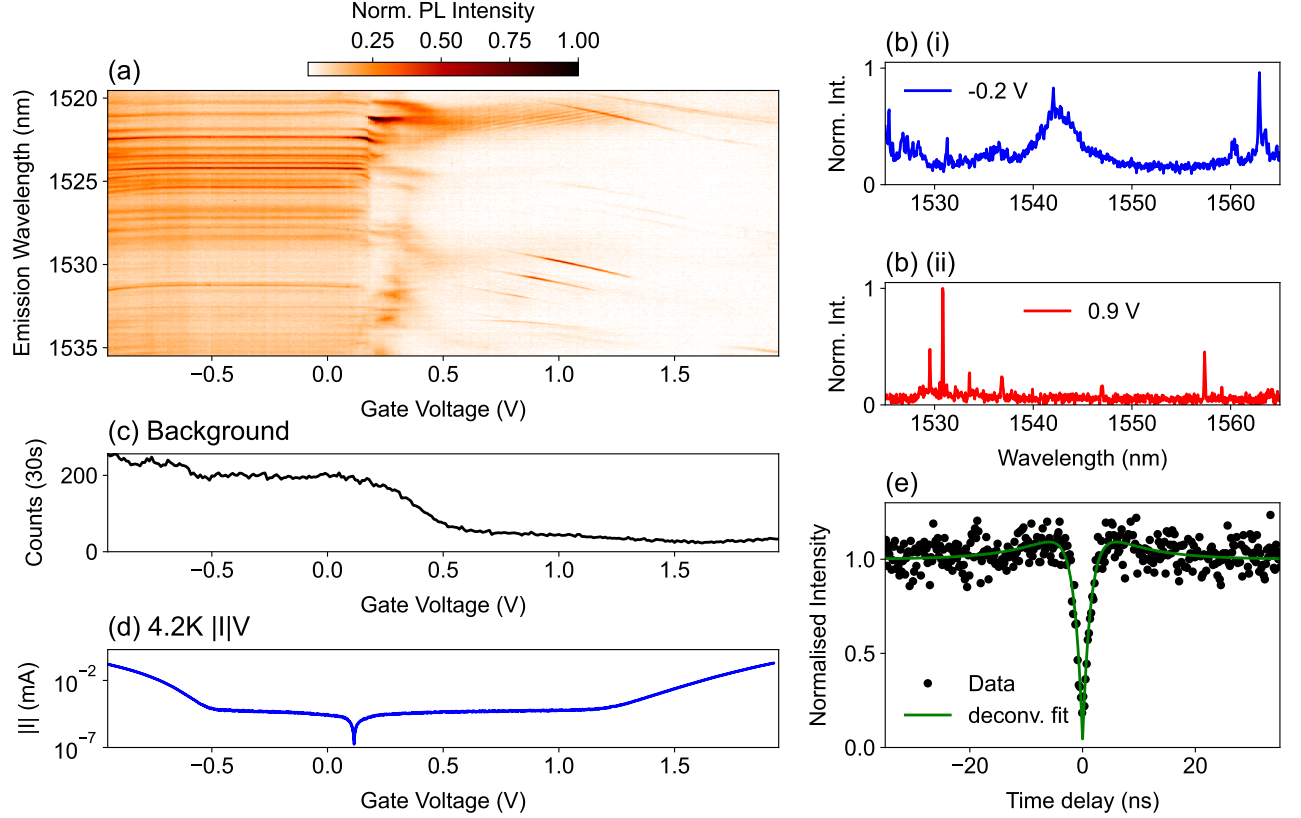


FIG. 2. (a) PL for $80 \mu\text{W}$ excitation as a function of applied bias voltage for a QD, showing voltage dependent tuning of QD lines in C-band (b) Representative normalized PL spectra from (a) for (i) high background -0.2 V bias voltage and (ii) low background 0.9 V gate voltage. (c) Average background count level with above band excitation of the sample at $80 \mu\text{W}$ power at different gate voltages (d) $|I|/V$ characteristics of the measured device at 4.2 K (with $30 \mu\text{W}$ of above-band (852 nm) excitation power). (e) HBT measurement confirming high purity single-photon emission from the QD at a gate voltage of 1.18 V and emission wavelength of 1530.3 nm . The normalized second-order correlation function $g^{(2)}(\tau)$ exhibits a clear anti-bunching dip at $\tau = 0$. Fitting yields $g^{(2)}(0) = 0.04 \pm 0.04$.

function of V_{gate} and the emission energy, revealing transitions between the neutral excitonic species (X^0) and singly charged (X^-) excitonic species. To verify the charge states and excitonic behavior, we measured both the fine-structure splitting (FSS) and power dependence for each highlighted state in Fig 3(a). Neutral excitonic species exhibit FSS due to exchange interactions between electron and hole spin states [46]. In contrast, the additional electron in X^- suppresses this interaction and therefore the emission line displays no FSS. The presence and degree of FSS was identified through polarization-dependent measurements, in which a linear polarizer in the collection path was rotated. Fig 3(b) shows the results of these measurements, where for a range of angles of the linear polarizer ($0 - 360^\circ$), the energy of the intensity peak of the PL was determined. The FSS was then calculated as the energy separation between the minimum and maximum energy across the range of angles. Fig 3(b, i-ii) show FSS indicating neutral states, while (iii) shows no appreciable FSS indicating the emission

line corresponds to a charged state. Considering the relative binding energies of the states [47], (iii) was determined to be a negatively charged trion (X^-). Additionally, we used power dependent PL measurements to identify single and biexcitonic emission lines. Because biexciton formation requires two e-h pairs, its PL intensity increases roughly twice as much as a single exciton for the same increase in excitation power [48]. Fig 3(c) shows the PL intensities of each state at excitation powers ranging from $5 \mu\text{W}$ to $360 \mu\text{W}$ (using an 850 nm continuous wave (CW) diode laser). Each peak was fit to determine the maximum PL as a function of external applied excitation power. The extracted slopes of: 0.78 , 0.88 , and 1.51 for X^- , X^0 , and XX , respectively, indicating a ~ 1.8 greater slope for XX compared to X^0 .

The application of an external electric field enables the continuous, reversible tuning of the emission wavelength of QDs [49, 50]. The tuning range for the three exciton states (operating within a signal-to-background ratio of 5:1), was determined by sweeping the gate volt-

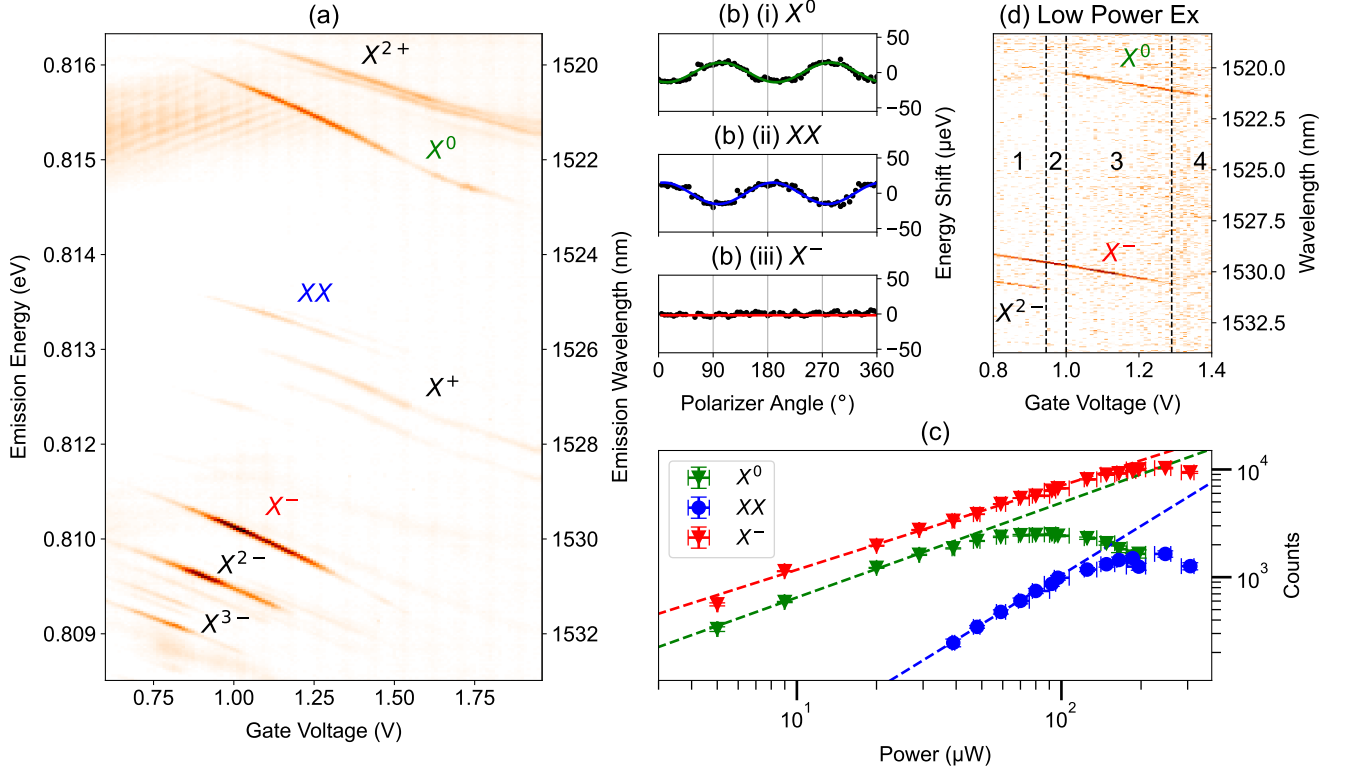


FIG. 3. (a) Micro-PL of a single selected QD as a function of gate voltage, using an above-barrier pumping scheme, in the low background gate voltage regime. (b) Polarization dependent PL of the (i) X^0 , (ii) XX and the X^- (iii) emission lines at 1.1 V gate voltage. The emission lines in (i-ii) exhibit polarization-dependent shifts arising from their intrinsic fine-structure splitting, their converse polarization dependence confirm a direct radiative cascade. (c) PL intensity as a function of excitation power for the X^0 , XX and X^- states. The dashed lines represent the power-dependent fit before dot saturation. (d) PL intensity spectra under weak above-band pumping (7% of saturation) of the QD for different applied gate voltages. For specific voltage regions, 2 and 4, only the X^0 or the X^- are present respectively.

age from 0.59 V to 1.96 V. We extract the tuning ranges of 2.40 nm, 0.82 nm and 1.73 nm for the X^0 , X^- and XX lines, respectively (see Section supplementary section S1). Such spectral control is indispensable for integrating QD emitters into scalable photonic networks, where frequency matching across multiple sources is crucial [51].

The ability to control the QD charge state is important in understanding the QD's level structure and has practical applications in spin-based quantum information processes [52]. Charge control enables precise initialization and readout of spin states [1], the foundational elements for spin-photon interfaces [53]. To clearly distinguish each excitonic transition in the PL, we employed a low-power, above-band optical excitation. Under these conditions, each charge configuration emerges in different gate voltage ranges, avoiding higher power phenomena such as substantial space-charge build-up or excessive spectral broadening [3, 53, 54]. The PL as a function of the gate voltage in this weak excitation regime is shown in Fig. 3(d), where four gate-voltage regimes can be distinguished: in Region 4 (1.3–1.4 V) the QD is neutral and

emits only the X^0 line; in Region 3 (1.0–1.29 V) both X^0 and X^- transitions appear; in Region 2 (0.945–1.0 V) the X^- line dominates as the QD holds an excess electron, suppressing X^0 ; and in Region 1 (0.8–0.945 V) the doubly charged exciton X^{2-} is observed, indicating higher electron occupancy. These regions correspond to the sequential charging of the QD through the Coulomb blockade regime, enabling clear identification of each excitonic transition under weak excitation [3, 53, 54].

Moreover, in the QD tuning range, the application of the electric field is also capable of reducing the FSS [55], a critical capability to preserve high-fidelity polarization entanglement in the biexciton-exciton cascade [27, 28, 56]. The FSS results from breaking the QD symmetry, in physical shape, composition, or strain terms [56]. Since such asymmetries are ubiquitous, in situ FSS tuning methods are essential for realizing high-fidelity entangled single-photon sources. Electrical tuning can reduce the FSS by reversing the overlap of the electron and hole wavefunctions that occurs as a result of the asymmetries. Other established methods for controlling the FSS include the application of stress [57–59] and magnetic

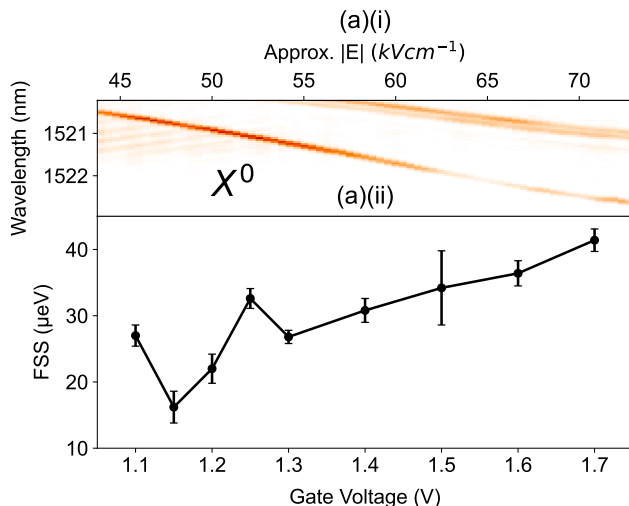


FIG. 4. (a)(i) PL Intensity of the X^0 state and (ii) Measurements of the fine structure splitting as a function of the applied gate voltage.

fields [60]. To demonstrate electrical control over the degree of FSS in our system, we performed polarization-resolved PL spectroscopy to measure the QD's FSS as a function of voltage. Fig. 4(i) shows the X^0 PL intensity as a function of gate voltage, with (ii) showing the corresponding measurement of the FSS as a function of gate voltage. Additionally the magnitude of the electric field is estimated for a $d_i = 240$ nm intrinsic region ($E = V/d_i$), across this voltage range. The extracted FSS ranges from $41 \pm 2 \mu\text{eV}$ at 1.7 V to $16 \pm 2 \mu\text{eV}$ at 1.15 V. This result underscores the viability of this system for telecom wavelength entangled SPS.

DISCUSSION AND OUTLOOK

In this work, we have introduced and validated an $n^{++}-i-n^+$ InP diode containing droplet epitaxy InAs QDs, demonstrating tunable single-photon generation at telecom wavelengths. Our results establish this structure as a promising platform for key quantum technologies. A principal advantage of this n-type gating scheme is its ability to mitigate p-dopant diffusion, a common issue in InP-based devices, thus opening the way to stabilizing the charge environment around each QD. By generating photons in the telecom C-band, future devices will be able to leverage the existing fiber infrastructure for practical quantum communication [61], while reduced fiber attenuation at C-band specifically benefits secure data links and distributed quantum computing.

The observed Stark shifts exceeding 2.4 nm confirm a useful single QD emission tuning range. Reliable tuning of a QD's emission wavelength is crucial for several key functionalities in quantum photonics. First, by finely

adjusting the QD's transition into resonance with a high quality factor cavity mode, one can exploit the Purcell effect to achieve ultrafast, deterministic single-photon emission [62], directional emission [63] and, in the strong-coupling regime, engineer zero-dimensional polaritons with well-defined energy splitting and lifetimes [64, 65]. Second, precise spectral alignment between two spatially separated QDs enables coherent dipole-dipole coupling [66, 67] or the emission of indistinguishable photons for entanglement protocols, both of which demand sub-meV tuning accuracy to overcome inhomogeneous broadening and fabrication variability. Finally, matching the QD's emission to narrow atomic transitions (e.g., the ORCA memory at 1529.3 nm [68]) allows deterministic storage and retrieval of single-photons in atomic ensembles [68], thereby forming a hybrid quantum node that combines solid-state emitters with long-lived atomic memories.

Furthermore, robust control over X^0 and X^- states highlights the potential of the device for spin-photon interfaces [40, 69, 70]. The demonstrated charge control opens possibilities for spin-based memory [71, 72] and quantum logic [73], where spin pumping [74] and coherent spin readout [75] at C-band could support quantum gates and small-scale entanglement on the same platform. Our demonstration of tunable single-photon emission in the telecom band thus marks a key milestone toward scalable quantum photonic circuits, and continued integration efforts and system-level demonstrations will further unlock the potential of these devices for quantum communication and computation at telecom wavelengths.

DATA AVAILABILITY

Data underlying the results presented in this article are not publicly available at this time, but may be obtained from the authors upon reasonable request.

ACKNOWLEDGMENTS

This work was supported by EPSRC Grant No. EP/V026496/1 and the Integrated Quantum Network Hub EP/Z533208/1. A.J.B. acknowledges additional support from the EPSRC (UK) fellowship EP/W027909 and the Royal Society Research Grant RG/R2/232470. The authors acknowledge helpful discussions with Dr Andrew Foster and Dr Mahmoud Jalali Mehrabad.

AUTHOR CONTRIBUTIONS

N.J.M. conceived the project, designed the electronic structure of the wafer, and together with A.J.B. oversaw the experimental work. N.J.M., A.J.B., A.T., C.L.P.,

L.H., P.M.-H., E.O.M., and D.H. carried out the experimental measurements. E.M.S. grew the QD wafer. R.D. performed device fabrication. E.O.M. and K.A.O. carried out the band structure simulations. J.H., M.S.S., A.M.F. and L.R.W. provided supervision and expertise. N.J.M., A.T. and E.O.M. wrote the manuscript with input from all authors.

COMPETING INTERESTS

The authors declare that they have no competing interests.

ASSOCIATED CONTENT

See Supplement 1 for supporting content.

* n.j.martin@sheffield.ac.uk

- [1] T. Heindel, J. H. Kim, N. Gregersen, A. Rastelli, and S. Reitzenstein, Quantum dots for photonic quantum information technology, *AOP* **15**, 613 (2023).
- [2] D. A. Vajner, L. Rickert, T. Gao, K. Kaymazlar, and T. Heindel, Quantum communication using semiconductor quantum dots, *Adv. Quant. Technol.* **5**, 2100116 (2022).
- [3] Y. Arakawa and M. J. Holmes, Progress in quantum-dot single photon sources for quantum information technologies: A broad spectrum overview, *Appl. Phys. Rev.* **7** (2020).
- [4] R. Singh and R. M. Bodile, A quick guide to quantum communication, *arXiv preprint arXiv:2402.15707* (2024).
- [5] J. Preskill, Quantum computing 40 years later, in *Feynman Lectures on Computation* (CRC Press, 2023) pp. 193–244.
- [6] H. Defienne, W. P. Bowen, M. Chekhova, G. B. Lemos, D. Oron, S. Ramelow, N. Treps, and D. Faccio, Advances in quantum imaging, *Nature Photonics* **18**, 1024 (2024).
- [7] P. Michler, *Single Semiconductor Quantum Dots* (Springer, 2009).
- [8] X. Cao, M. Zopf, and F. Ding, Telecom wavelength single photon sources, *J. Semicond.* **40**, 071901 (2019).
- [9] L. Schweickert, K. D. Jöns, K. D. Zeuner, S. F. Covre da Silva, H. Huang, T. Lettner, M. Reindl, J. Zichi, R. Trotta, A. Rastelli, *et al.*, On-demand generation of background-free single photons from a solid-state source, *Appl. Phys. Lett.* **112**, 093106 (2018).
- [10] P. Michler and S. L. Portalupi, *Semiconductor Quantum Light Sources: Fundamentals, Technologies and Devices* (Walter de Gruyter GmbH & Co KG, 2024).
- [11] S. Gyger, K. D. Zeuner, T. Lettner, S. Bensoussan, M. Carläs, L. Ekemar, L. Schweickert, C. R. Hedlund, M. Hammar, T. Nilsson, *et al.*, Metropolitan single-photon distribution at 1550 nm for random number generation, *Appl. Phys. Lett.* **121** (2022).
- [12] M. Paul, F. Olbrich, J. Höschle, S. Schreier, J. Kettler, S. L. Portalupi, M. Jetter, and P. Michler, Single-photon emission at 1.55 μm from MOPVE-grown InAs quantum dots on InGaAs/GaAs metamorphic buffers, *Appl. Phys. Lett.* **111** (2017).
- [13] F. Olbrich, J. Höschle, M. Müller, J. Kettler, S. Luca Portalupi, M. Paul, M. Jetter, and P. Michler, Polarization-entangled photons from an InGaAs-based quantum dot emitting in the telecom C-band, *Appl. Phys. Lett.* **111** (2017).
- [14] K. Takemoto, Y. Nambu, T. Miyazawa, Y. Sakuma, T. Yamamoto, S. Yorozu, and Y. Arakawa, Quantum key distribution over 120 km using ultrahigh purity single-photon source and superconducting single-photon detectors, *Sci. Rep.* **5**, 14383 (2015).
- [15] T. Miyazawa, K. Takemoto, Y. Nambu, S. Miki, T. Yamashita, H. Terai, M. Fujiwara, M. Sasaki, Y. Sakuma, M. Takatsu, *et al.*, Single-photon emission at 1.5 μm from an InAs/InP quantum dot with highly suppressed multi-photon emission probabilities, *Appl. Phys. Lett.* **109** (2016).
- [16] A. N. Wakileh, L. Yu, D. Dokuz, S. Haffouz, X. Wu, J. Lapointe, D. B. Northeast, R. L. Williams, N. Rotenberg, P. J. Poole, *et al.*, Single photon emission in the telecom C-band from nanowire-based quantum dots, *Appl. Phys. Lett.* **124**, 044006 (2024).
- [17] T. Müller, J. Skiba-Szymanska, A. Krysa, J. Huwer, M. Felle, M. Anderson, R. Stevenson, J. Heffernan, D. A. Ritchie, and A. Shields, A quantum light-emitting diode for the standard telecom window around 1,550 nm, *Nat. Commun.* **9**, 862 (2018).
- [18] A. Jaffal, W. Redjem, P. Regreny, H. S. Nguyen, S. Cuff, X. Letartre, G. Patriarche, E. Rousseau, G. Cassaboïs, M. Gendry, and N. Chauvin, Inas quantum dot in a needlelike tapered inP nanowire: a telecom band single photon source monolithically grown on silicon, *Nanoscale* **11**, 21847 (2019).
- [19] S. Haffouz, K. D. Zeuner, D. Dalacu, P. J. Poole, J. Lapointe, D. Poitras, K. Mnaymneh, X. Wu, M. Couillard, M. Korkusinski, *et al.*, Bright single InAsP quantum dots at telecom wavelengths in position-controlled InP nanowires: the role of the photonic waveguide, *Nano Lett.* **18**, 3047 (2018).
- [20] G. Bucci, V. Zannier, F. Rossi, A. Musiał, J. Boniecki, G. Şek, and L. Sorba, Zincblende inasxp1-x/inP quantum dot nanowires for telecom wavelength emission, *ACS Applied Materials and Interfaces* **16**, 26491 (2024).
- [21] R. Joos, S. Bauer, C. Rupp, S. Kolatschek, W. Fischer, C. Nawrath, P. Vijayan, R. Sittig, M. Jetter, S. L. Portalupi, *et al.*, Coherently and Incoherently Pumped Telecom C-Band Single-Photon Source with High Brightness and Indistinguishability, *Nano Lett.* **24**, 8626 (2024).
- [22] Z. Ge, T. Chung, Y.-M. He, M. Benyoucef, and Y. Huo, Polarized and bright telecom C-band single-photon source from InP-based quantum dots coupled to elliptical Bragg gratings, *Nano Lett.* **24**, 1746 (2024).
- [23] P. Holewa, D. A. Vajner, E. Zieba-Ostój, M. Wasiluk, B. Gaál, A. Sakanas, M. Burakowski, P. Mrowiński, B. Krajník, M. Xiong, *et al.*, High-throughput quantum photonic devices emitting indistinguishable photons in the telecom C-band, *Nat. Commun.* **15**, 3358 (2024).
- [24] J. Kim, J. Kaupp, Y. Reum, G. Peniakov, J. Michl, F. Kohr, M. Emmerling, M. Kamp, Y.-H. Cho, T. Huber-Loyola, S. Höfling, and A. T. Pfenning, Two-Photon Interference from an InAs Quantum Dot emitting in the Telecom C-Band, *arXiv preprint* (2025),

- arXiv:2501.15970 [quant-ph].
- [25] C. Nawrath, F. Olbrich, M. Paul, S. Portalupi, M. Jetter, and P. Michler, Coherence and indistinguishability of highly pure single photons from non-resonantly and resonantly excited telecom c-band quantum dots, *Appl. Phys. Lett.* **115** (2019).
 - [26] N. Ha, T. Mano, S. Dubos, T. Kuroda, Y. Sakuma, and K. Sakoda, Single photon emission from droplet epitaxial quantum dots in the standard telecom window around a wavelength of 1.55 μm , *Applied Physics Express* **13**, 025002 (2020).
 - [27] P. Laccotripes, T. Müller, R. Stevenson, J. Skiba-Szymanska, D. Ritchie, and A. Shields, Spin-photon entanglement with direct photon emission in the telecom C-band, *arXiv preprint arXiv:2310.16930* (2023).
 - [28] M. Anderson, T. Müller, J. Huwer, J. Skiba-Szymanska, A. Krysa, R. Stevenson, J. Heffernan, D. Ritchie, and A. Shields, Quantum teleportation using highly coherent emission from telecom C-band quantum dots, *npj Quantum Inf.* **6**, 14 (2020).
 - [29] M. Anderson, T. Müller, J. Skiba-Szymanska, A. Krysa, J. Huwer, R. Stevenson, J. Heffernan, D. Ritchie, and A. Shields, Coherence in single photon emission from droplet epitaxy and Stranski–Krastanov quantum dots in the telecom C-band, *Appl. Phys. Lett.* **118** (2021).
 - [30] C. L. Phillips, A. J. Brash, M. Godsland, N. J. Martin, A. Foster, A. Tomlinson, R. Dost, N. Babazadeh, E. M. Sala, L. Wilson, *et al.*, Purcell-enhanced single photons at telecom wavelengths from a quantum dot in a photonic crystal cavity, *Sci. Rep.* **14**, 4450 (2024).
 - [31] L. Wells, T. Müller, R. Stevenson, J. Skiba-Szymanska, D. Ritchie, and A. Shields, Coherent light scattering from a telecom C-band quantum dot, *Nat. Commun.* **14**, 8371 (2023).
 - [32] J. Kaupp, Y. Reum, F. Kohr, J. Michl, Q. Buchinger, A. Wolf, G. Peniakov, T. Huber-Loyola, A. Pfenning, and S. Höfling, Purcell-Enhanced Single-Photon Emission in the Telecom C-Band, *Adv. Quantum Technol.* **6**, 2300242 (2023).
 - [33] J. Skiba-Szymanska, R. M. Stevenson, C. Varnava, M. Felle, J. Huwer, T. Müller, A. J. Bennett, J. P. Lee, I. Farrer, A. B. Krysa, *et al.*, Universal growth scheme for quantum dots with low fine-structure splitting at various emission wavelengths, *Phys. Rev. Appl.* **8**, 014013 (2017).
 - [34] E. M. Sala, Y. I. Na, M. Godsland, A. Trapalis, and J. Heffernan, InAs/InP quantum dots in etched pits by droplet epitaxy in metalorganic vapor phase epitaxy, *Phys. Status Solidi RRL* **14**, 2000173 (2020).
 - [35] E. M. Sala, M. Godsland, A. Trapalis, and J. Heffernan, Effect of cap thickness on InAs/InP quantum dots grown by droplet epitaxy in metal–organic vapor phase epitaxy, *Phys. Status Solidi RRL* **15**, 2100283 (2021).
 - [36] E. M. Sala, M. Godsland, Y. I. Na, A. Trapalis, and J. Heffernan, Droplet epitaxy of InAs/InP quantum dots via MOVPE by using an InGaAs interlayer, *Nanotechnology* **33**, 065601 (2022).
 - [37] E. M. Sala, Y. I. Na, M. Godsland, and J. Heffernan, Self-Assembled InAs Quantum Dots on InGaAsP/InP (100) by Modified Droplet Epitaxy in Metal–Organic Vapor Phase Epitaxy around the Telecom C-Band for Quantum Photonic Applications, *Phys. Status Solidi RRL* **18**, 2300340 (2024).
 - [38] P. Holewa, S. Kadkhodazadeh, M. Gawelczyk, P. Baluta, A. Musiał, V. G. Dubrovskii, M. Syperek, and E. Semenova, Droplet epitaxy symmetric InAs/InP quantum dots for quantum emission in the third telecom window: morphology, optical and electronic properties, *Nanophotonics* **11**, 1515 (2022).
 - [39] R. Uppu, F. T. Pedersen, Y. Wang, C. T. Olesen, C. Papon, X. Zhou, L. Midolo, S. Scholz, A. D. Wieck, A. Ludwig, and P. Lodahl, Scalable integrated single-photon source, *Science Advances* **6**, eabc8268 (2020), <https://www.science.org/doi/pdf/10.1126/sciadv.abc8268>.
 - [40] N. Somaschi, V. Giesz, L. D. Santis, J. C. Loredó, M. P. Almeida, G. Hornecker, S. L. Portalupi, T. Grange, C. Antón, J. Demory, C. Gómez, I. Sagnes, N. D. Lanzillotti-Kimura, A. Lemaître, A. Auffeves, A. G. White, L. Lanco, and P. Senellart, Near-optimal single-photon sources in the solid state, *Nature Photonics* **2016** **10**, 340 (2016).
 - [41] D. A. Vajner, P. Holewa, E. Zięba-Ostoja, M. Wasiluk, M. von Helversen, A. Sakanas, A. Huck, K. Yvind, N. Gregersen, A. Musiał, *et al.*, On-demand generation of indistinguishable photons in the telecom C-band using quantum dot devices, *ACS photonics* **11**, 339 (2024).
 - [42] A. Barbiero, G. Shooter, J. Skiba-Szymanska, J. Huang, L. Ravi, J. I. Davies, B. Ramsay, D. J. P. Ellis, A. J. Shields, T. Müller, and R. M. Stevenson, *Purcell enhanced and tunable single-photon emission at telecom wavelengths from inas quantum dots in circular photonic crystal resonators* (2025), [arXiv:2505.11069 \[physics.optics\]](https://arxiv.org/abs/2505.11069).
 - [43] T. Strobel, J. H. Weber, M. Schmidt, L. Wagner, L. Engel, M. Jetter, A. D. Wieck, S. L. Portalupi, A. Ludwig, and P. Michler, A unipolar quantum dot diode structure for advanced quantum light sources, *Nano Letters* **23**, 6574 (2023), pMID: 37432064, <https://doi.org/10.1021/acs.nanolett.3c01658>.
 - [44] F. T. Pedersen, Y. Wang, C. T. Olesen, S. Scholz, A. D. Wieck, A. Ludwig, M. C. Löbl, R. J. Warburton, L. Midolo, R. Uppu, and P. Lodahl, Near transform-limited quantum dot linewidths in a broadband photonic crystal waveguide, *ACS Photonics* **7**, 2343 (2020).
 - [45] J. Casey, H. C., D. D. Sell, and K. W. Wecht, Concentration dependence of the absorption coefficient for n- and p-type gaas between 1.3 and 1.6 eV, *Journal of Applied Physics* **46**, 250 (1975), https://pubs.aip.org/aip/jap/article-pdf/46/1/250/18369402/250_1_online.pdf.
 - [46] M. Bayer, G. Ortner, O. Stern, A. Kuther, A. A. Gorbunov, A. Forchel, P. Hawrylak, S. Fafard, K. Hinzer, T. L. Reinecke, S. N. Walck, J. P. Reithmaier, F. Kloppe, and F. Schäfer, Fine structure of neutral and charged excitons in self-assembled In(Ga)As/(Al)GaAs quantum dots, *Phys. Rev. B* **65**, 195315 (2002).
 - [47] G. Peniakov, J. Michl, M. Helal, R. Joos, M. Jetter, S. L. Portalupi, P. Michler, S. Höfling, and T. Huber-Loyola, Initialization of neutral and charged exciton spin states in a telecom-emitting quantum dot, *arXiv preprint arXiv:2504.20497* (2025).
 - [48] J. Kettler, M. Paul, F. Olbrich, K. Zeuner, M. Jetter, P. Michler, M. Florian, C. Carmesin, and F. Jahnke, Neutral and charged biexciton-exciton cascade in near-telecom-wavelength quantum dots, *Physical Review B* **94**, 045303 (2016).

- [49] A. Högele, S. Seidl, M. Kroner, K. Karrai, R. J. Warburton, B. D. Gerardot, and P. M. Petroff, Voltage-controlled optics of a quantum dot, *Phys. Rev. Lett.* **93**, 217401 (2004).
- [50] A. K. Nowak, S. L. Portalupi, V. Giesz, O. Gazzano, C. Dal Savio, P.-F. Braun, K. Karrai, C. Arnold, L. Lanco, I. Sagnes, A. Lemaître, and P. Senellart, Deterministic and electrically tunable bright single-photon source, *Nature Communications* **5**, 3240 (2014).
- [51] S. Slussarenko and G. J. Pryde, Photonic quantum information processing: A concise review, *Applied Physics Reviews* **6**, 041303 (2019).
- [52] M. Ediger, P. Dalgarno, J. Smith, B. Gerardot, R. Warburton, K. Karrai, and P. Petroff, Controlled generation of neutral, negatively-charged and positively-charged excitons in the same single quantum dot, *Applied Physics Letters* **86** (2005).
- [53] R. J. Warburton, Single spins in self-assembled quantum dots, *Nature Materials* **12**, 483 (2013).
- [54] M. C. Löbl, I. Söllner, A. Javadi, T. Pregnotato, R. Schott, L. Midolo, A. V. Kuhlmann, S. Stobbe, A. D. Wieck, P. Lodahl, A. Ludwig, and R. J. Warburton, Narrow optical linewidths and spin pumping on charge-tunable close-to-surface self-assembled quantum dots in an ultrathin diode, *Phys. Rev. B* **96**, 165440 (2017).
- [55] A. J. Bennett, M. A. Pooley, R. M. Stevenson, M. B. Ward, R. B. Patel, A. B. D. L. Giroday, N. Sköld, I. Farrer, C. A. Nicoll, D. A. Ritchie, and A. J. Shields, Electric-field-induced coherent coupling of the exciton states in a single quantum dot, *Nature Physics* **2010** 6:12 **6**, 947 (2010).
- [56] L. He, M. Gong, C. F. Li, G. C. Guo, and A. Zunger, Highly reduced fine-structure splitting in InAs/InP quantum dots offering an efficient on-demand entangled 1.55- μm photon emitter, *Physical Review Letters* **101**, 157405 (2008).
- [57] S. Seidl, M. Kroner, A. Högele, K. Karrai, R. J. Warburton, A. Badolato, and P. M. Petroff, Effect of uniaxial stress on excitons in a self-assembled quantum dot, *Applied Physics Letters* **88**, 203113 (2006).
- [58] R. Trotta, J. Martín-Sánchez, J. S. Wildmann, G. Piredda, M. Reindl, C. Schimpf, E. Zallo, S. Stroj, J. Edlinger, and A. Rastelli, Wavelength-tunable sources of entangled photons interfaced with atomic vapours, *Nature Communications* **2016** 7:1 **7**, 1 (2016).
- [59] P. Millington-Hotze, H. E. Dyte, S. Manna, S. F. C. da Silva, A. Rastelli, and E. A. Chekhovich, Approaching a fully-polarized state of nuclear spins in a solid, *Nature Communications* **2024** 15:1 **15**, 1 (2024).
- [60] R. M. Stevenson, R. J. Young, P. See, D. G. Gevaux, K. Cooper, P. Atkinson, I. Farrer, D. A. Ritchie, and A. J. Shields, Magnetic-field-induced reduction of the exciton polarization splitting in InAs quantum dots, *Physical Review B - Condensed Matter and Materials Physics* **73**, 033306 (2006).
- [61] T. E. Northup and R. Blatt, Quantum information transfer using photons, *Nature Photonics* **2014** 8:5 **8**, 356 (2014).
- [62] F. Liu, A. J. Brash, J. O'Hara, L. M. P. P. Martins, C. L. Phillips, R. J. Coles, B. Royall, E. Clarke, C. Benthams, N. Prtljaga, I. E. Itskevich, L. R. Wilson, M. S. Skolnick, and A. M. Fox, High purcell factor generation of indistinguishable on-chip single photons, *Nature Nanotechnology* **13**, 835 (2018).
- [63] N. J. Martin, D. Hallett, M. Duda, L. Hallacy, E. Callus, L. Brunswick, R. Dost, E. Clarke, P. K. Patil, P. Kok, M. S. Skolnick, and L. R. Wilson, *Purcell-enhanced, directional light-matter interaction in a waveguide-coupled nanocavity* (2025), [arXiv:2501.10351 \[physics.optics\]](https://arxiv.org/abs/2501.10351).
- [64] A. Laucht, F. Hofbauer, N. Hauke, J. Angele, S. Stobbe, M. Kaniber, G. Böhm, P. Lodahl, M.-C. Amann, and J. J. Finley, Electrical control of spontaneous emission and strong coupling for a single quantum dot, *New Journal of Physics* **11**, 023034 (2009).
- [65] A. Faraon, A. Majumdar, H. Kim, P. Petroff, and J. Vučković, Fast electrical control of a quantum dot strongly coupled to a photonic-crystal cavity, *Phys. Rev. Lett.* **104**, 047402 (2010).
- [66] D. Hallett, J. Wiercinski, L. Hallacy, S. Sheldon, R. Dost, N. Martin, A. Fenzl, I. Farrer, A. Verma, M. Cygorek, E. M. Gauger, M. S. Skolnick, and L. R. Wilson, *Controlling coherence between waveguide-coupled quantum dots* (2025), [arXiv:2410.17890 \[quant-ph\]](https://arxiv.org/abs/2410.17890).
- [67] A. Tiranov, V. Angelopoulou, C. J. van Diepen, B. Schirnski, O. A. D. Sandberg, Y. Wang, L. Midolo, S. Scholz, A. D. Wieck, A. Ludwig, A. S. Sørensen, and P. Lodahl, Collective super- and subradiant dynamics between distant optical quantum emitters, *Science* **379**, 389 (2023).
- [68] S. E. Thomas, L. Wagner, R. Joos, R. Sittig, C. Nawrath, P. Burdakin, I. M. de Buy Wenniger, M. J. Rasiah, T. Huber-Loyola, S. Sagana-Stophel, S. Höfling, M. Jetter, P. Michler, I. A. Walmsley, S. L. Portalupi, and P. M. Ledingham, Deterministic storage and retrieval of telecom light from a quantum dot single-photon source interfaced with an atomic quantum memory, *Science Advances* **10**, eadi7346 (2024).
- [69] P. Lodahl, S. Mahmoodian, and S. Stobbe, Interfacing single photons and single quantum dots with photonic nanostructures, *Reviews of Modern Physics* **87**, 347 (2015).
- [70] A. V. Kuhlmann, J. Houel, A. Ludwig, L. Greuter, D. Reuter, A. D. Wieck, M. Poggio, and R. J. Warburton, Charge noise and spin noise in a semiconductor quantum device, *Nature Physics* **2013** 9:9 **9**, 570 (2013).
- [71] S. Sun, H. Kim, Z. Luo, G. S. Solomon, and E. Waks, A single-photon switch and transistor enabled by a solid-state quantum memory, *Science* **361**, 57 (2018).
- [72] J. Dreiser, M. Atatüre, C. Galland, T. Müller, A. Badolato, and A. Imamoglu, Optical investigations of quantum dot spin dynamics as a function of external electric and magnetic fields, *Physical Review B - Condensed Matter and Materials Physics* **77**, 075317 (2008).
- [73] L. De Santis, C. Antón, B. Reznichenko, N. Somaschi, G. Coppola, J. Senellart, C. Gómez, A. Lemaître, I. Sagnes, A. G. White, L. Lanco, A. Auffèves, and P. Senellart, A solid-state single-photon filter, *Nature Nanotechnology* **12**, 663 (2017).
- [74] S. G. Carter, T. M. Sweeney, M. Kim, C. S. Kim, D. Solenov, S. E. Economou, T. L. Reinecke, L. Yang, A. S. Bracker, and D. Gammon, Quantum control of a spin qubit coupled to a photonic crystal cavity, *Nature Photonics* **2013** 7:4 **7**, 329 (2013).
- [75] N. O. Antoniadis, M. R. Hogg, W. F. Stehl, A. Javadi, N. Tomm, R. Schott, S. R. Valentin, A. D. Wieck, A. Ludwig, and R. J. Warburton, Cavity-enhanced single-shot readout of a quantum dot spin within 3 nanoseconds, *Nature Communications* **2023** 14:1 **14**, 1

- (2023).
- [76] D. Caughey and R. Thomas, Carrier mobilities in silicon empirically related to doping and field, *Proceedings of the IEEE* **55**, 2192 (1967).
 - [77] S. Selberherr, A. Schutz, and H. Potzl, Minimos - a two-dimensional mos transistor analyzer, *IEEE Journal of Solid-State Circuits* **15**, 605 (1980).
 - [78] I. Vurgaftman, J. R. Meyer, and L. R. Ram-Mohan, Band parameters for iii-v compound semiconductors and their alloys, *Journal of Applied Physics* **89**, 5815 (2001).
 - [79] P. Aivaliotis, L. R. Wilson, E. A. Zibik, J. W. Cockburn, M. J. Steer, and H. Y. Liu, Enhancing the dot density in quantum dot infrared photodetectors via the incorporation of antimony, *Applied Physics Letters* **91**, 013503 (2007), https://pubs.aip.org/aip/apl/article-pdf/doi/10.1063/1.2753727/13669707/013503_1_online.pdf.
 - [80] A. D. Stiff, S. Krishna, P. Bhattacharya, and S. Kennerly, High-detectivity, normal-incidence, mid-infrared ($\lambda \sim 4\mu\text{m}$) InAs/GaAs quantum-dot detector operating at 150 K, *Applied Physics Letters* **79**, 421 (2001), https://pubs.aip.org/aip/apl/article-pdf/79/3/421/18559248/421_1_online.pdf.
 - [81] S. J. Xu, S. J. Chua, T. Mei, X. C. Wang, X. H. Zhang, G. Karunasiri, W. J. Fan, C. H. Wang, J. Jiang, S. Wang, and X. G. Xie, Characteristics of ingaas quantum dot infrared photodetectors, *Applied Physics Letters* **73**, 3153 (1998), https://pubs.aip.org/aip/apl/article-pdf/73/21/3153/18537740/3153_1_online.pdf.
-

Supplementary information: Stark Tuning and Charge State Control in Individual C-Band Quantum Dots

S1.TUNING FITTING

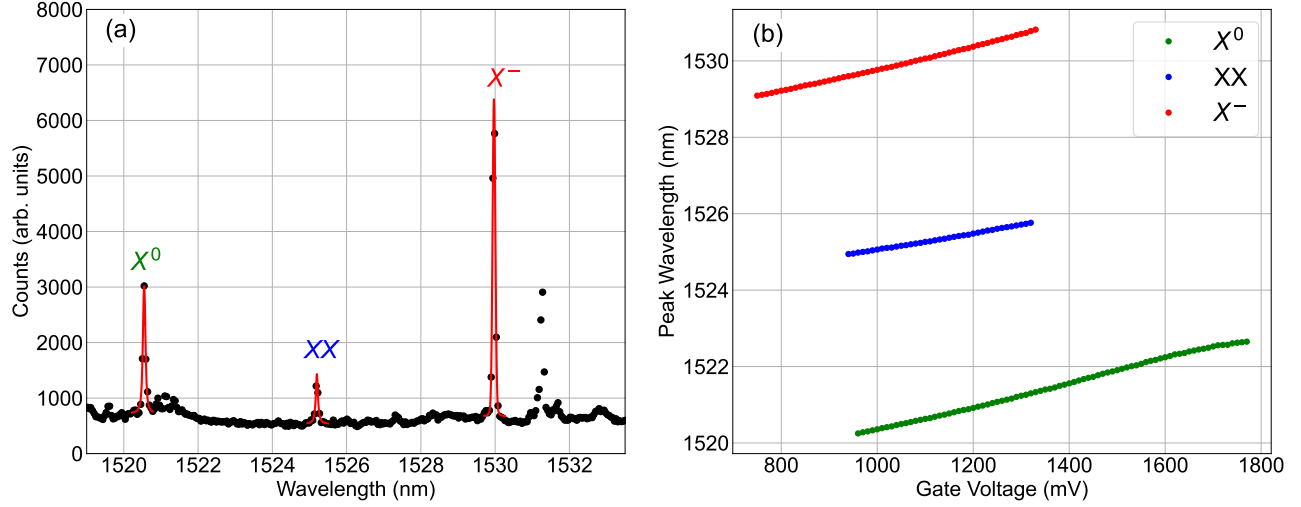


FIG. S1. (a) Photoluminescence (PL) measurements at a gate voltage of 1.07 V. (b) Tuning plots for each excitonic state.

To determine the exact tuning range for the three excitonic states, PL measurements were performed at $100 \mu\text{W}$ with voltages ranging between 0.59 V and 1.96 V. A fit was applied to each peak and the peak wavelength extracted. At a gate voltage of 1.07 V, Fig. S1(a) demonstrates the fitting for each state. To ensure accurate peak fitting, a signal-to-background ratio fitting constraint of 5 was applied, discarding peaks below this threshold. Fig. S1(b) shows the fitted peak wavelength as a function of gate voltage, resulting in tuning ranges of 2.40, 0.82 and 1.73 nm for the X^0 , XX and X^- states respectively.

S2. 300K HETEROSTRUCTURE BAND STRUCTURES

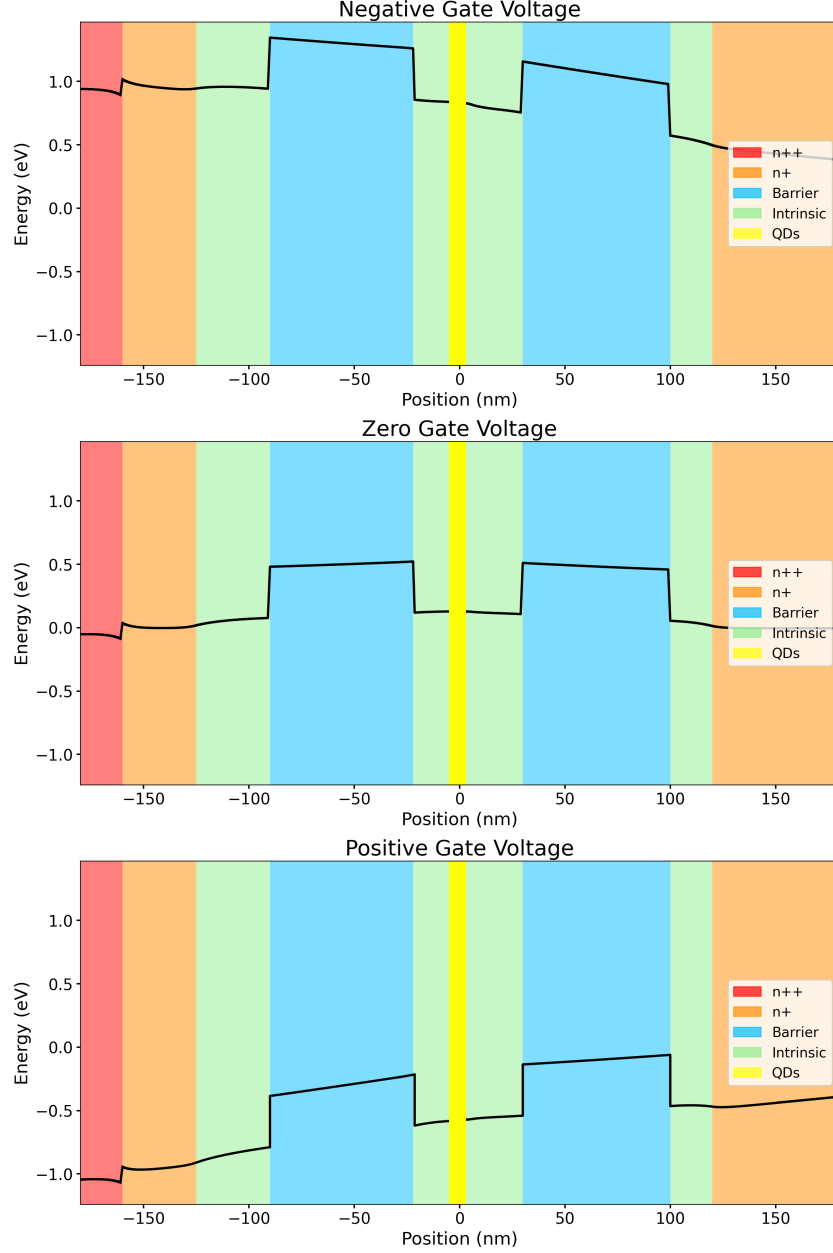


FIG. S2. Simulated band structures of the sample at different applied biases at 300 K. The black line represents the conduction band.

To characterize the band structures of our diode, a 1D model of the device was coded in Nextnano (nextnano.com), from which the bandedges were computed using the Nextnano current-Poisson solver. This was performed for a sweep of applied biases to determine how the band structure changes with the applied voltage. Fig. S2 shows an expected shift in band energy as a function of voltage. The background doping levels for the intrinsic and barrier layers were $(2.0 \times 10^{15} \text{ cm}^{-3})$ and $(7.0 \times 10^{14} \text{ cm}^{-3})$ respectively. For the doping of the n+ and n++ regions, see results section and Fig. 1. This simulation uses material properties at 300 K and uses the MINIMOS doping dependent carrier mobility model [76, 77]. The material parameters in the Nextnano database, taken from Vurgaftman (2001) [78], were used in this simulation.

S3. IV CHARACTERISTICS

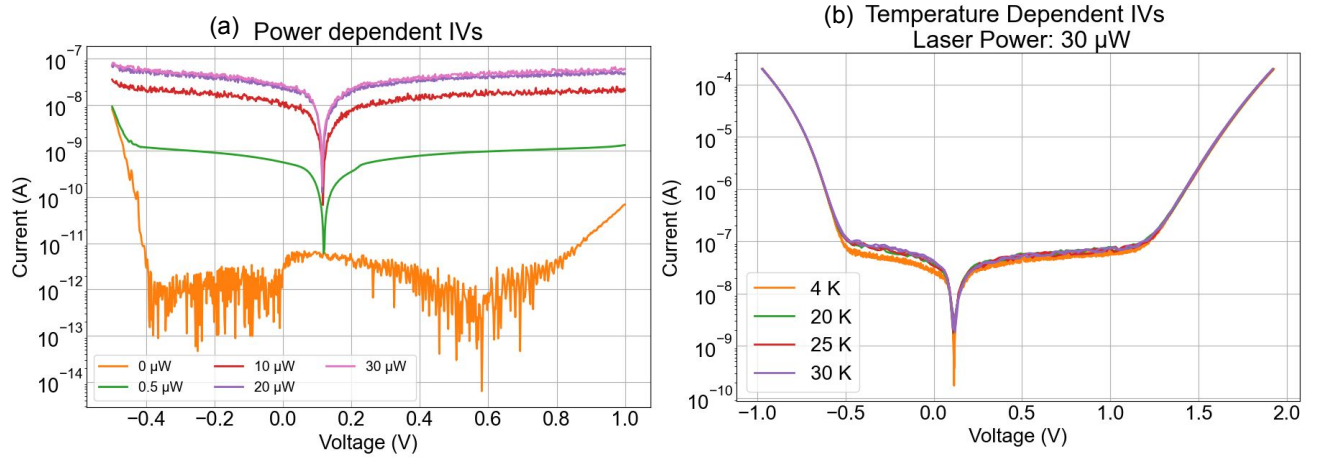


FIG. S3. (a) IV characteristics of the n-i-n heterostructure measured at 4 K under increasing above-band (852 nm) excitation power (0 μW to 30 μW). The dip-like feature near 0.2 V is also visible in Fig. 2(d). (b) IV curves recorded at 30 temperatures from 4 K up to 30 K, using an embedded resistive heater. The dark IV characteristics are consistent with those of other similar n-i-n QD structures, such as quantum dot infrared photo detectors (QDIPS) [79–81]. In such structures, asymmetries in the IV characteristics are associated with asymmetry in the device structure, such as barrier thickness and doping profile.

S4. PL LIFETIME

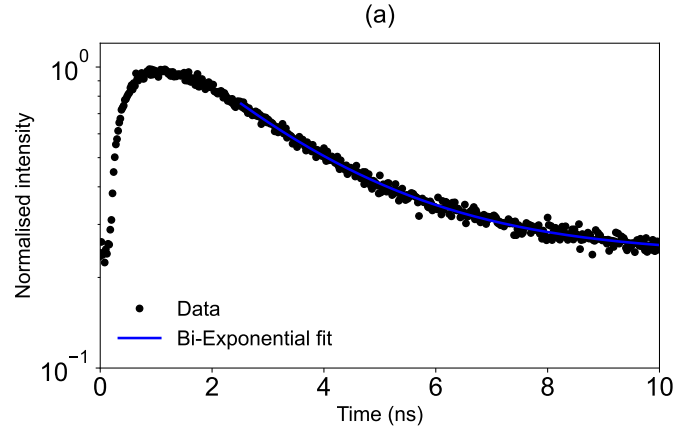


FIG. S4. Time-resolved photoluminescence measurement of QD under pulsed excitation at a gate voltage of 1.18 V. The decay curve is well described by a bi-exponential fit (solid line), yielding an exciton lifetime of approximately $\tau \approx 2.2$ ns.

Fig S4 shows a time-resolved photoluminescence measurement of the X^- state at 1.18 V and under pulsed 830 nm excitation. The measurement reveals a biexponential decay profile, with a principal exciton lifetime of approximately $\tau \approx 2.2$ ns. The shorter and longer components likely reflect distinct recombination pathways or a combination of radiative and non-radiative processes typical for this excitation scheme [30].